Dexmedetomidine Disrupts the Local and Global Efficiencies of Large-scale Brain Networks

Javeria A. Hashmi, Ph.D., Marco L. Loggia, Ph.D., Sheraz Khan, Ph.D., Lei Gao, M.D., Jieun Kim, Ph.D., Vitaly Napadow, Ph.D., Emery N. Brown, M.D., Ph.D., Oluwaseun Akeju, M.D., M.M.Sc.

ABSTRACT

Background: A clear understanding of the neural basis of consciousness is fundamental to research in clinical and basic neuroscience disciplines and anesthesia. Recently, decreased efficiency of information integration was suggested as a core network feature of propofol-induced unconsciousness. However, it is unclear whether this finding can be generalized to dexmedetomidine, which has a different molecular target.

Methods: Dexmedetomidine was administered as a 1-μg/kg bolus over 10 min, followed by a $0.7\text{-}\mu g \cdot kg^{-1} \cdot h^{-1}$ infusion to healthy human volunteers (age range, 18 to 36 yr; n = 15). Resting-state functional magnetic resonance imaging data were acquired during baseline, dexmedetomidine-induced altered arousal, and recovery states. Zero-lag correlations between resting-state functional magnetic resonance imaging signals extracted from 131 brain parcellations were used to construct weighted brain networks. Network efficiency, degree distribution, and node strength were computed using graph analysis. Parcellated brain regions were also mapped to known resting-state networks to study functional connectivity changes.

Results: Dexmedetomidine significantly reduced the local and global efficiencies of graph theory–derived networks. Dexmedetomidine also reduced the average brain connectivity strength without impairing the degree distribution. Functional connectivity within and between all resting-state networks was modulated by dexmedetomidine.

Conclusions: Dexmedetomidine is associated with a significant drop in the capacity for efficient information transmission at both the local and global levels. These changes result from reductions in the strength of connectivity and also manifest as reduced within and between resting-state network connectivity. These findings strengthen the hypothesis that conscious processing relies on an efficient system of information transfer in the brain. (**ANESTHESIOLOGY 2017; 126:419-30**)

UNDERSTANDING the neural basis of consciousness is fundamental to research in clinical and basic neuroscience disciplines and anesthesia.[1] However, we are yet to clearly decipher how the human brain mediates consciousness. This is because the brain is a complex biologic system composed of components that interact dynamically to give rise to higher brain functions.[2,3] For example, the sensory experience of a painfully hot object comprises various composite experiences[4] (*i.e.*, intensity, duration, quality, and emotional distress) that are integrated by the brain and represented as a unified experience of pain.[2,3,5–9]

Synchronization of resting-state functional magnetic resonance imaging (rsfMRI) slow signals is a proxy for the putative neural syntax that integrates various brain regions into networks mediating higher brain functions.[10–13] Numerous investigations of anesthesia-induced changes to rsfMRI networks have been conducted. For a review, see Hudetz.[14] However, less studied is how anesthetics alter the capacity of information transfer in rsfMRI brain networks, and how this relates to the brain state in question. This graph-theoretic

What We Already Know about This Topic

- Decreased efficiency in information integration has been suggested as a core network feature of propofol-induced unconsciousness. However, it is unclear whether this finding can be generalized to anesthetics with different molecular targets.

What This Article Tells Us That Is New

- Using resting-state functional magnetic resonance in healthy human volunteers, it was shown that dexmedetomidine significantly reduced the local and global efficiencies of graph theory–derived networks, reduced the mean strength of network connectivity without impairing the degree distribution, and modulated functional connectivity within and between all resting-state networks.

- These findings strengthen the hypothesis that conscious processing relies on an efficient system of information transfer in the brain.

approach, which is distinct from standard functional connectivity analyses, is based on the fundamental premise that the brain is topologically organized to maximize information transfer within and between networks.[15,16] This approach

<zdoi;10.1097/ALN.0000000000001509>

parallels theories of consciousness that stress integrated information processing.[8,9]

Network efficiency is a graph-theoretical measure of information exchange. A recent study of the γ-aminobutyric acid receptor agonist propofol described decreased efficiency of information transfer as a key differentiating feature of conscious and unconscious brain states.[17] Similarly, decreased efficiency of information transfer has also been suggested to account for decreased consciousness during nonrapid eye movement sleep.[18,19] Thus, altered states of arousal may be associated with network reconfigurations that favor decreased efficiency of communication. However, the generalizability of this finding is unclear. Thus, studies of anesthetics from different drug classes are necessary to help refine our knowledge of information processing correlates of unconsciousness.

Using a graph-theoretical approach, we studied network changes associated with dexmedetomidine, an α2-adrenergic agonist that activates endogenous sleep pathways.[20–24] We hypothesized that dexmedetomidine would result in decreased capacity for information integration as represented by surrogate markers of local and global network communication (local and global efficiencies). Furthermore, we hypothesized that this decrease in information integration results from reduced synchronization strength between brain regions. In a previous study, we found that dexmedetomidine preferentially decreased blood flow and metabolism in the thalamus, default mode network, and bilateral frontoparietal networks.[1] Therefore, we also hypothesized that between-network disruption in these and other resting-state networks (RSNs) is associated with dexmedetomidine.

To explore these hypotheses, blood oxygen level–dependent (BOLD) signals obtained during baseline, dexmedetomidine-induced altered arousal, and recovery states were analyzed (n = 15, 18 to 36 yr of age). Zero-lag correlations between rsfMRI signals extracted from 131 brain parcellations were used to construct weighted brain networks. Network efficiency and node strength were computed using graph analysis. Parcellated brain regions were also mapped to known RSNs (table 1). This data set was previously reported in a within-network analysis of the default mode and frontoparietal networks.[1]

Materials and Methods

Imaging Visit

The Human Research Committee at the Massachusetts General Hospital (Boston, Massachusetts) approved this study (protocol no. 2011P002333; clinical trial no. NCT01485380). Written informed consent was obtained after the nature and possible study consequences of the study were explained to each healthy volunteer (18 to 36 yr; n = 15). All volunteers were required to be American Society of Anesthesiologists Physical Status I. Brain imaging was performed with the Biograph mMR scanner (Siemens Healthcare, Germany), which allows simultaneous acquisition of whole-body positron emission tomography and 3-Tesla magnetic resonance imaging data. At the beginning of the imaging visit, structural magnetic resonance imaging (magnetization-prepared rapid acquisition with gradient echo volume, repetition time/echo time = 2,100/3.24 ms; flip angle = 7°, voxel size = 1 mm isotropic) was acquired for the purpose of anatomical localization and spatial normalization of the imaging data. BOLD functional magnetic resonance imaging data were collected using a whole-brain T2*-weighted gradient echo BOLD; echo planar imaging pulse sequence was used (repetition time/echo time = 3,000/35 ms, flip angle = 90°, voxel size = 2.3 × 2.3 × 3.8 mm, number of slices = 35).

Dexmedetomidine was administered as a 1-μg/kg loading bolus over 10 min, followed by a $0.7\text{-}\mu g \cdot kg^{-1} \cdot h^{-1}$ infusion. During the infusion period, an anesthesiologist monitored cuff blood pressure, capnography, electrocardiogram, and pulse oximetry. Volunteers were instructed to keep their eyes open during the course of the study. During the start of the dexmedetomidine infusion (*i.e.*, bolus), a 20-min *induction* pulsed arterial spin label (pASL) scan was acquired. Altered arousal was defined as the onset of sustained eye closure and the lack of response to a verbal request to open the eyes at 1-min intervals during the induction pASL scan. Sustained eye closure and the lack of response to verbal stimuli were confirmed in all subjects during the induction pASL. The dexmedetomidine-induced altered arousal BOLD rsfMRI scans were acquired after the induction pASL scan. At the end of the dexmedetomidine infusion, a 20-min *recovery* pASL scan was also acquired. During this period, arousal was also periodically assessed verbally at 1-min intervals. Spontaneous eye opening and a positive response to give a thumbs-up signal were used to determine recovery. Arousability to the verbal stimulus was confirmed in all subjects during the 20-min recovery pASL scan. The recovery BOLD rsfMRI scan was acquired after the pASL scan. The resting-state nature of our data acquisition precluded continuous assessments of arousal during rsfMRI BOLD data acquisition.

Data Preprocessing

Both FMRIB Software Library v5.0 (FSL, University of Oxford, United Kingdom) and Analysis of Functional Neuro-Images (National Institute of Mental Health Scientific and Statistical Computing Core, USA) software were used to preprocess data in line with procedures adapted for the 1,000 Functional Connectomes project.[25] Data were slice-time corrected for interleaved acquisitions using Fourier interpolation, motion corrected using least squares alignment of each volume to the eighth image using Fourier interpolation, despiked of extreme time series outliers using a continuous transformation function, temporal band-pass filtered between 0.009 and 0.3 Hz using Fourier transformation, and further filtered to remove linear and quadratic trends using analysis of functional neuro-images. In addition, FSL was used for spatially smoothing the images (Gaussian kernel full width half maximum = 6 mm) and for normalizing the mean-based intensity by the same factor (10,000). Next, eight nuisance signals (time courses of white matter and cerebrospinal fluid, and

Table 1. Resting-state Networks, Anatomic Brain Regions, and Associated Montreal Neurological Institute Coordinates

Networks	Regions	Abbreviations	MNI Coordinates		
			x	y	z
1	Brain stem	BrStem	0	−26	−28
1	Amygdala right	Amyg_R	24	−4	−18
1	Caudate right	Caud_R	12	12	10
1	Globus pallidus right	GP_R	16	−2	−2
1	Hippocampus right	Hipp_R	28	−22	−16
1	Nucleus accumbens right	NAc_R	10	10	−8
1	Putamen right	Put_R	20	−4	0
1	Thalamus right	Thal_R	10	−18	8
1	Thalamus left	Thal_L	10	−18	8
1	Putamen left	Put_L	−20	−4	0
1	Nucleus accumbens left	NAc_L	−10	10	−8
1	Hippocampus left	Hipp_L	−28	−22	−16
1	Globus pallidus left	GP_L	−16	−2	−2
1	Caudate left	Caud_L	−12	14	8
1	Amygdala left	Amyg_L	−24	−4	−18
2	Central opercular cortex right	Cop_R	48	−4	8
2	Dorsal anterior insula right	dINSa_R	32	20	0
2	Middle insula right	INSm_R	40	−2	−2
2	Posterior insula right	INSp_R	38	−14	8
2	Postcentral gyrus right	PostC_R	54	−20	46
2	Precentral gyrus right	PreC_R	44	−8	52
2	Supra marginal gyrus right	SMGa_R	58	32	40
2	Ventral anterior insula right	vINSa_R	36	10	−14
2	Temporal occipital fusiform cortex right	TOF_R	34	−54	−16
2	Temporal fusiform cortex, posterior division right	TFCp_R	36	−16	−32
2	Planum polare right	PIP_R	48	−4	−6
2	Planum temporale right	PIT_R	60	−22	8
2	Heschls gyrus (includes H1 and H2) right	He_R	48	−18	−6
2	Cuneal cortex right	Cun_R	4	−82	30
2	Intracalcarine cortex right	IC_R	6	−68	12
2	Lateral occipital cortex, inferior division right	LOcci_R	48	−78	−2
2	Lateral occipital cortex, superior division right	LOccs_R	40	−78	34
2	Occipital fusiform gyrus right	OccFG_R	28	−76	−14
2	Occipital pole right	OccP_R	8	−100	6
2	Precuneous cortex right	pCun_R	4	−64	38
2	Supracalcarine cortex right	Sc_R	2	−84	12
2	Supracalcarine cortex left	Sc_L	−2	−84	12
2	Precuneous cortex left	pCun_L	−4	−82	30
2	Occipital pole left	OccP_L	−8	−100	6
2	Occipital fusiform gyrus left	OccFG_L	−28	−76	−14
2	Lateral occipital cortex, superior division left	LOccs_L	−40	−78	34
2	Lateral occipital cortex, inferior division left	LOcci_L	−48	−78	−2
2	Intracalcarine cortex left	IC_L	−28	−76	−14
2	Cuneal cortex left	Cun_L	−6	−74	12
2	Heschls gyrus (includes H1 and H2) left	He_L	−48	−18	6
2	Planum temporale left	PIT_L	−60	−22	8
2	Planum polare left	PIP_L	−48	−4	−6
2	Temporal fusiform cortex, posterior division left	TFCp_L	−36	−16	−32
2	Temporal occipital fusiform cortex left	TOF_L	−34	−54	−16
2	Ventral anterior insula left	vINSa_L	−36	10	−14
2	Supra marginal gyrus left	SMGa_L	−54	−56	26
2	Precentral gyrus left	PreC_L	−44	−8	52
2	Postcentral gyrus left	PostC_L	−58	32	40
2	Posterior insula left	INSp_L	−38	−14	8
2	Middle insula left	INSm_L	−40	−2	−2

(Continued)

421

Table 1. *(Continued)*

Networks	Regions	Abbreviations	MNI Coordinates		
			x	*y*	*z*
2	Dorsal anterior insula left	dINSa_L	−32	20	0
2	Central opercular cortex left	Cop_L	−48	−4	8
3	Caudal anterior cingulate right	ACCc_R	4	40	−2
3	Rostral anterior cingulate mid posterior right	ACCrm_R	−6	60	8
3	Rostral anterior cingulate posterior right	ACCrp_R	−6	−2	42
3	Rostral anterior cingulate right	ACCr_R	2	28	18
3	Subgenual anterior cingulate right	ACCsg_R	4	16	−14
3	Dorsal medial prefrontal cortex, anterior division right	dMPFCa_R	4	50	28
3	Frontal orbital cortex right	FO_R	40	20	4
3	Medial prefrontal cortex right	MPFC_R	6	60	8
3	Ventral medial prefrontal cortex right	vMPFC_R	4	50	−20
3	Angular gyrus right	Ang_R	54	−56	26
3	Cingulate gyrus, posterior division right	Cingp_R	4	−38	32
3	Cingulate gyrus, posterior division left	Cingp_L	−4	−38	32
3	Angular gyrus left	Ang_L	−48	−4	8
3	Ventral medial prefrontal cortex left	vMPFC_L	−4	50	−20
3	Medial prefrontal cortex left	MPFC_L	−6	60	8
3	Frontal orbital cortex left	FO_L	−40	30	−14
3	Dorsal medial prefrontal cortex, anterior division left	dMPFCa_L	−4	50	28
3	Subgenual anterior cingulate left	ACCsg_L	−2	28	18
3	Rostral anterior cingulate posterior left	ACCrp_L	6	18	34
3	Rostral anterior cingulate mid posterior left	ACCrm_L	20	28	18
3	Rostral anterior cingulate left	ACCr_L	−6	18	34
3	Caudal anterior cingulate left	ACCc_L	−4	40	−2
4	Frontal pole right	FP_R	30	54	20
4	Orbito frontal pole right	OFP_R	32	58	−6
4	Superior frontal gyrus right	SFG_R	20	18	62
4	Middle frontal gyrus right	MFG_R	40	20	44
4	Supramarginal gyrus, posterior division right	SMGp_R	60	−48	32
4	Superior parietal lobule right	SPL_R	32	−50	60
4	Mid anterior cingulate right	ACCm_R	6	−2	42
4	Dorsal medial prefrontal cortex, posterior division right	dMPFCp_R	4	26	48
4	Frontal operculum cortex right	Fop_R	−48	−32	20
4	Inferior frontal gyrus, pars opercularis right	IFGpo_R	54	14	16
4	Inferior frontal gyrus, pars triangularis right	IFGpt_R	−50	30	16
4	Parietal operculum cortex right	Pop_R	48	−32	20
4	Supplementary motor area right	SMA_R	4	−2	58
4	Supplementary motor area left	SMA_L	−4	−2	58
4	Parietal operculum cortex left	Pop_L	−38	4	0
4	Inferior frontal gyrus, pars triangularis left	IFGpt_L	−50	30	16
4	Inferior frontal gyrus, pars opercularis left	IFGpo_L	−54	−20	46
4	Inferior frontal gyrus, pars opercularis left	Fop_L	40	30	−14
4	Dorsal medial prefrontal cortex, posterior division left	dMPFCp_L	−4	26	48
4	Mid anterior cingulate left	ACCm_L	−4	50	−20
4	Superior parietal lobule left	SPL_L	−60	−48	32
4	Supramarginal gyrus, posterior division left	SMGp_L	−40	20	4
4	Middle frontal gyrus left	MFG_L	−40	20	44
4	Superior frontal gyrus left	SFG_L	−22	22	54
4	Orbito frontal pole left	OFP_L	−32	58	−6
4	Frontal pole left	FP_L	−30	54	20
5	Temporal pole right	TP_R	40	16	−30
5	Superior temporal gyrus, anterior division right	STGa_R	58	−4	−6
5	Superior temporal gyrus, posterior division right	STGp_R	66	−26	6
5	Temporal fusiform cortex, anterior division right	TFCa_R	32	−6	−42

(Continued)

Table 1. *(Continued)*

Networks	Regions	Abbreviations	MNI Coordinates		
			x	*y*	*z*
5	Parahippocampal gyrus, anterior division right	pHippa_R	34	−6	−34
5	Parahippocampal gyrus, posterior division right	pHippp_R	34	−32	−18
5	Inferior temporal gyrus, anterior division right	ITGa_R	50	−6	−40
5	Inferior temporal gyrus, posterior division right	ITGp_R	56	−32	−24
5	Inferior temporal gyrus, temporooccipital part right	ITGtp_R	56	−54	−18
5	Lingual gyrus right	Ling_R	10	−68	−2
5	Middle temporal gyrus, anterior division right	MTGa_R	58	−2	−22
5	Middle temporal gyrus, posterior division right	MTGp_R	66	−22	12
5	Middle temporal gyrus, temporooccipital part right	MTGto_R	60	−52	0
5	Middle temporal gyrus, temporooccipital part left	MTGto_L	−60	−52	0
5	Middle temporal gyrus, posterior division left	MTGp_L	−66	−22	12
5	Middle temporal gyrus, anterior division left	MTGa_L	−58	−2	−22
5	Lingual gyrus left	Ling_L	−10	−68	−2
5	Inferior temporal gyrus, temporooccipital part left	ITGtp_L	−56	−54	−18
5	Inferior temporal gyrus, posterior division left	ITGp_L	−56	−32	−24
5	Inferior temporal gyrus, anterior division left	ITGa_L	−50	−6	−40
5	Parahippocampal gyrus, posterior division left	pHippp_L	−34	−32	−18
5	Parahippocampal gyrus, anterior division left	pHippa_L	−34	−6	−34
5	Temporal fusiform cortex, anterior division left	TFCa_L	−32	−6	−42
5	Superior temporal gyrus, posterior division left	STGp_L	−66	−26	6
5	Superior temporal gyrus, anterior division left	STGa_L	−58	−4	−6
5	Temporal pole left	TP_L	−40	16	−30

MNI = Montreal Neurological Institute.

six motion parameters) were used as regressors of no interest. White matter and cerebrospinal fluid time series were extracted from masks obtained by segmenting each individual's high-resolution structural image using FMRIB's Automated Segmentation Tool (University of Oxford, United Kingdom), thresholded at 80% tissue-type probability. The six motion parameters were generated in the FSL-based motion correction step. These six vectors included rotational movement around three axes (pitch, yaw, and roll) and movement in each of the three cardinal directions (X, Y, and Z). All of these steps were conducted in native functional space.

For registration, FMRIB's Linear and Non-LINEAR Image Registration Tools were used for transformations from native functional and structural space to the Montreal Neurological Institute (Montréal, Quebec, Canada) MNI152 template with $2 \times 2 \times 2$ mm resolution. First, the high-resolution structural image was registered to the MNI152 2-mm template with a 12 degrees of freedom linear affine transformation. The transformation was further refined using FMRIB's Non-LINEAR Image Registration Tool. Next, each participant's functional data were registered to their high-resolution structural image using a linear transformation with 6 degrees of freedom. The structural-to-standard nonlinear transformation matrix was used to register the functional volume to MNI152 standard space.

Brain Parcellation and Time Course Extraction

The brain was anatomically parcellated using a previously published parcellation scheme.[26] Briefly, the Harvard Oxford

Atlas was refined by increasing the anatomical partitioning of the cingulate, medial, and lateral prefrontal cortices. In addition, anatomical partitioning of the insular label was also performed. Thus, instead of the single region of interest spanning the entire insula in the Harvard Oxford Atlas, the insula was subdivided into posterior, middle, dorsal anterior, and ventral anterior regions based on a previously published scheme.[27] Regions spanning the right and left hemispheres were separated to create hemisphere-specific regions. The complete parcellation scheme consisted of a total of 131 regions (table 1). A list of these regions, their coordinates, and a description of the anatomical landmarks used for the subdivision of the Harvard Oxford labels in smaller parcellates have previously been published.[26] Each region of interest was designated as a node. Thus, from each node, the BOLD time series were extracted and averaged to generate a 131 time series for each subject.

RSN Network Construction

Each parcellated brain region or node was classified as belonging to a designated RSN based on spatial overlap with a specific RSN map. The RSN maps were identified using functional connectivity maps in the neurosynth framework (last accessed February 15, 2016).[28] Each region was represented in only one RSN, based on maximum overlap.

Graph Analysis

Whole-brain networks were constructed and network measures were assessed using the Brain Connectivity Toolbox

(MATLAB, USA).[29] For each patient, the BOLD time series in each region was correlated with every other region to create a 131×131 weighted connectivity or adjacency matrix. The adjacency matrices were thresholded at connectivity densities of 0.05, 0.1, 0.15, 0.2, 0.25, and 0.3. The following graph functions were computed from each matrix:

Strength. This function measures the strength of connections in the graph. Node strength is the sum of weights of links connected to the node.

$$str = sum(CIJ)$$

where CIJ is the undirected weighted connection matrix. Mean connectivity strength of the graph was measured by averaging str from all nodes.

Global and Local Efficiencies. Efficiency is a measure of the network's capacity for parallel information transfer between nodes through multiple series of edges. The average global efficiency of information transfer in graph g having n nodes can be calculated from the inverse of the edge distances d_{ij}

$$E_{glob} = E(g) = \frac{1}{n(n-1)} \sum_{i \neq j; v_i, v_j \in g} \frac{1}{d_{ij}}$$

The quantity above is a measure of the global efficiency of information transfer for the whole graph g. There is also a local efficiency for each vertex v_i, measuring how efficiently its neighbors can communicate when vertex v_i is removed. If the subgraph of all neighbors of v_i is denoted by g_i, then its local efficiency $E(g_i)$ is approximately equivalent to the clustering coefficient C_i.[10]

$$E_{loc} = \frac{1}{n} \sum_{v_i \in g} E(g_i)$$

Statistical Comparisons

Comparison between the local and global efficiencies and the mean connectivity strength between the three states was first conducted using repeated-measures ANOVA (table 2). *Post hoc* comparisons were conducted on significant ANOVA findings using the paired t test. Significance was set at $P < 0.05$, and Bonferroni correction for multiple comparisons was employed. Statistics on graph results and graphical presentations of networks were performed with custom code written in MATLAB (USA).

RSN functional connectivity analyses were also conducted using custom code written in MATLAB. First, we present mean networks for the three conditions (awake, dexmedetomidine, and recovery). To assess statistical differences, each network was held at a threshold proportional to 50% of strongest connections, and these matrices were compared using a paired t test. Each test was corrected for multiple comparisons setting the false discovery rate to $P < 0.05$. The regions that showed significant changes in connectivity are shown as binarized maps where nodes are sorted based on membership to RSN groupings. To calculate the percentage of modulated connections within- and between-RSN networks as a discrete value, the total number of significantly modulated connections that survived correction for multiple comparisons were summed for within-RSN network and between-network connections.

This value was then divided by the number of total possible connections for any given combination and multiplied by one hundred to calculate the percentage of modulated connections. The final values were represented as a heat map to qualitatively assess network modulations.

Results

Dexmedetomidine Disrupts the Local and Global Efficiencies of Brain Networks

The local efficiency of weighted brain networks was significantly disrupted during the dexmedetomidine-induced altered arousal state compared to the awake state (fig. 1A; 0.15: $P = 0.003$, 0.2: $P = 0.004$, 0.25: $P = 0.004$, and 0.3: $P = 0.004$). During the recovery state, the local efficiency reverted to higher values compared to the dexmedetomidine-induced state. However, these findings did not meet our conservative Bonferroni-adjusted threshold for significance (fig. 1A; 0.15: $P = 0.03$, 0.2: $P = 0.029$, 0.25: $P = 0.029$, and 0.3: $P = 0.038$). There were no statistically significant differences between awake and recovery state comparisons (fig. 1A; $P > 0.025$).

The global efficiency of weighted brain networks was significantly disrupted during the dexmedetomidine-induced altered arousal state compared to the awake state (fig. 1B; 0.1: $P = 0.006$, 0.15: $P = 0.001$, 0.2: $P = 0.002$, 0.25: $P = 0.002$, and 0.3: $P = 0.002$). During the recovery state, the global efficiency was significantly increased for most, but not for all network thresholds (fig. 1B; 0.1: $P = 0.004$, 0.15: $P = 0.005$, 0.2: $P = 0.01$, 0.25: $P = 0.017$, and 0.3: $P = 0.026$). There were no statistically significant differences between awake and recovery state comparisons (fig. 1B; $P > 0.025$)

Dexmedetomidine Reduces the Strength of Synchronizations in Brain Networks

Next, using a graph-theoretic approach, a significant reduction in the mean strength of nodal connectivity was found during the dexmedetomidine-induced altered arousal state compared to the awake state (fig. 2A; 0.1: $P = 0.006$, 0.15: $P = 0.005$, 0.2: $P = 0.005$, 0.25: $P = 0.005$, and 0.3: $P = 0.005$). The recovery state was associated with increased mean strength of nodal connectivity compared to the dexmedetomidine-induced altered arousal state. However, this change in strength was not significant (fig. 2A; 0.05: $P = 0.052$, 0.1: $P = 0.051$, 0.15: $P = 0.053$, 0.2: $P = 0.055$, 0.25: = 0.055, and 0.3: $P = 0.056$). There were no statistically significant differences between awake and recovery state comparisons (fig. 2A; $P > 0.025$).

To study the nodes that principally contributed to the changes in the mean strength of connectivity, nodes were first sorted (from the lowest to the highest strength of connectivity during the awake state) and then plotted by the strength of connectivity (fig. 2B). The largest decreases in connectivity strength were most evident in strongly connected nodes. During the recovery state, the mean strength of connectivity

Table 2. Results from Repeated-measures ANOVA

Threshold	Mean	SD	F Value	P Value
Mean local efficiency				
0.05				
Awake	0.501	0.040	0.499	0.611
Dexmedetomidine	0.485	0.052		
Recovery	0.491	0.032		
0.1				
Awake	0.604	0.056	2.960	0.064
Dexmedetomidine	0.557	0.064		
Recovery	0.577	0.029		
0.15				
Awake	0.620	0.074	3.703	0.034
Dexmedetomidine	0.554	0.071		
Recovery	0.593	0.045		
0.2				
Awake	0.607	0.084	3.561	0.038
Dexmedetomidine	0.533	0.079		
Recovery	0.580	0.054		
0.25				
Awake	0.582	0.096	3.702	0.034
Dexmedetomidine	0.508	0.083		
Recovery	0.560	0.066		
0.3				
Awake	0.577	0.107	3.766	0.032
Dexmedetomidine	0.484	0.086		
Recovery	0.537	0.072		
Global efficiency				
0.05				
Awake	0.176	0.032	0.870	0.428
Dexmedetomidine	0.164	0.020		
Recovery	0.170	0.014		
0.1				
Awake	0.283	0.029	4.150	0.023
Dexmedetomidine	0.259	0.021		
Recovery	0.276	0.016		
0.15				
Awake	0.333	0.039	5.210	0.010
Dexmedetomidine	0.295	0.029		
Recovery	0.319	0.022		
0.2				
Awake	0.360	0.050	4.660	0.015
Dexmedetomidine	0.314	0.037		
Recovery	0.342	0.031		
0.25				
Awake	0.377	0.058	4.440	0.018
Dexmedetomidine	0.324	0.042		
Recovery	0.356	0.039		
0.3				
Awake	0.388	0.065	4.180	0.023
Dexmedetomidine	0.330	0.047		
Recovery	0.363	0.044		
Mean node strength				
0.05				
Awake	5.351	0.377	3.126	0.055
Dexmedetomidine	5.033	0.393		
Recovery	5.238	0.231		

(Continued)

Table 2. *(Continued)*

Threshold	Mean	SD	F Value	P Value
0.1				
Awake	9.916	1.002	3.510	0.040
Dexmedetomidine	9.025	0.984		
Recovery	9.564	0.659		
0.15				
Awake	14.031	1.768	3.589	0.037
Dexmedetomidine	12.470	1.633		
Recovery	13.380	1.185		
0.2				
Awake	17.792	2.632	3.602	0.037
Dexmedetomidine	15.500	2.306		
Recovery	16.801	1.776		
0.25				
Awake	21.257	3.573	3.603	0.037
Dexmedetomidine	18.192	2.982		
Recovery	19.893	2.415		
0.3				
Awake	24.449	4.577	3.587	0.037
Dexmedetomidine	20.586	3.649		
Recovery	22.690	3.089		

reverted to higher values compared to the dexmedetomidine-induced altered arousal state. The degree distribution (number of connection at each node) was studied to understand whether the changes in the strength of connectivity at the nodal level primarily resulted from a reduction in a number of connections *versus* a reduction in the strength of connection. Dexmedetomidine did not strongly modulate the number of connections at the nodal level (fig. 2C).

To graphically illustrate our results, plots of network graphs where nodes with common connections are plotted as clusters and the distances between nodes represent the strength of connectivity were made (fig. 2, D–F). This network representation more clearly depicts that changes in network strength of connections are a significant driver of topologic changes during the dexmedetomidine-induced altered arousal state.

Dexmedetomidine Alters Connection Within and Between Resting-state Networks

Parcellated brain regions were sorted based on composition to RSNs. During the dexmedetomidine-induced altered arousal state, the strength of connectivity within and between networks held at the same link density appeared different compared to the baseline and recovery states (fig. 3, A–C). Contrasts between the states were analyzed to characterize connectivity changes associated with dexmedetomidine (contrast 1: awake *vs.* dexmedetomidine; fig. 3D) and recovery (contrast 2: recovery *vs.* dexmedetomidine; fig. 3E). Although volunteers were responsive to verbal commands during the recovery period, they remained mildly sedated due to residual drug effects. Therefore, contrasts between the awake and recovery states (contrast 3: awake *vs.* recovery; fig. 3F) were also analyzed. Only connectivity changes in contrast 1 were
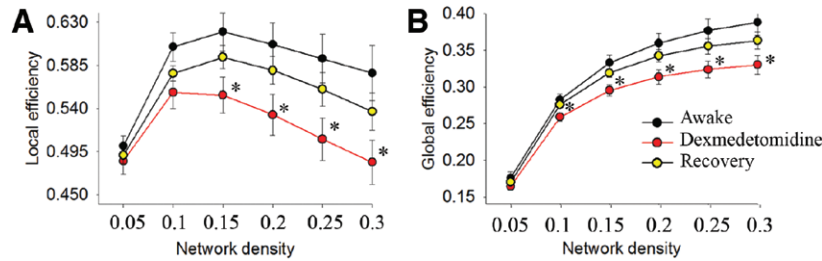
Fig. 1. Local and global efficiencies of neural information transfer are disrupted by dexmedetomidine (*A* and *B*). Local and global efficiencies are significantly decreased during the dexmedetomidine-induced altered arousal state and reverted to higher values during the recovery state. This observation was consistent at a range of network densities. *$P < 0.025$ for awake *vs.* dexmedetomidine, *error bars* represent ±SEM.

significant after correction for multiple comparisons. Therefore, corrected maps for contrast 1 and uncorrected maps ($P < 0.01$) for contrasts 2 and 3 are shown (fig. 3, D–F).

The percentages of modulated connections scaled by the total number of possible connections are presented for qualitative assessment (fig. 3, G–I). The dexmedetomidine-induced altered arousal state was associated with significant reductions in functional connectivity between regions that comprise all RSNs (fig. 3D; awake > dexmedetomidine; false discovery rate corrected $P < 0.05$). Recovery was associated with
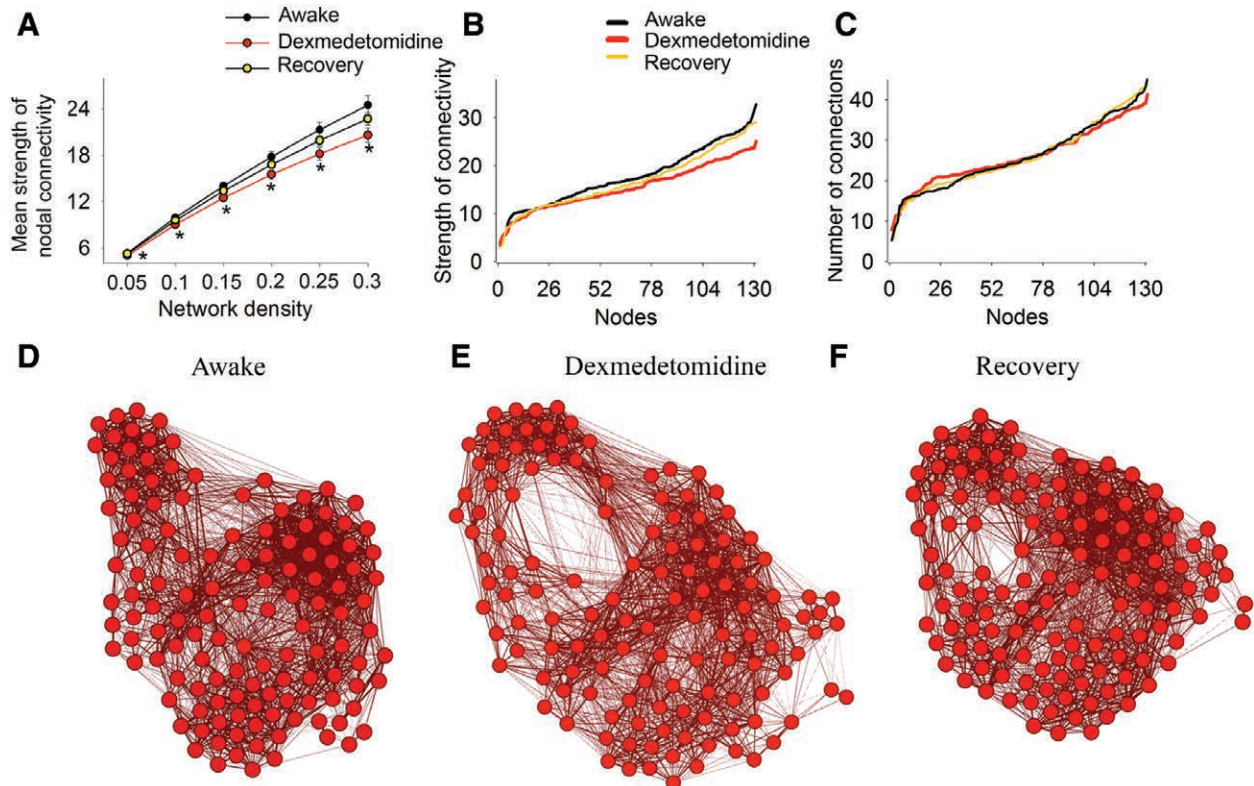
Fig. 2. Dexmedetomidine modulates the strength of connectivity in brain networks. (*A*) Mean strength of nodal connectivity in weighted networks reported for different network sparsities (*$P < 0.025$ for awake *vs.* dexmedetomidine, *error bars* represent ±SEM). (*B*) Mean strength of connection presented for each node. Nodes are ordered in ascending order of strength of connections to show that the most strongly connected nodes were the most disrupted by dexmedetomidine. (*C*) Mean degree (total number of connections) of each node is presented in ascending order. (*D–F*) Representations of large-scale network topology, illustrating how connectivity strength (weights) modulated by dexmedetomidine contributes to alterations in network architecture. The positioning of nodes is topologic rather than anatomical. The algorithm positions network nodes based on the strength of connections, so that regions with common connections are placed in a group and the physical distance between the nodes is adjusted based on the weight of the connection. The awake state shows an ordered modular structure with a large number of within-module connections. The modules are held together by global connections. In the dexmedetomidine-induced state, the strengths of connection (weights) are reduced at both the local (within-module) and global (between-module) levels. In the recovery state, the strength of connections is increased, but does not fully revert to the awake state. All three representative networks were constructed at a threshold proportional to 0.25 connections.
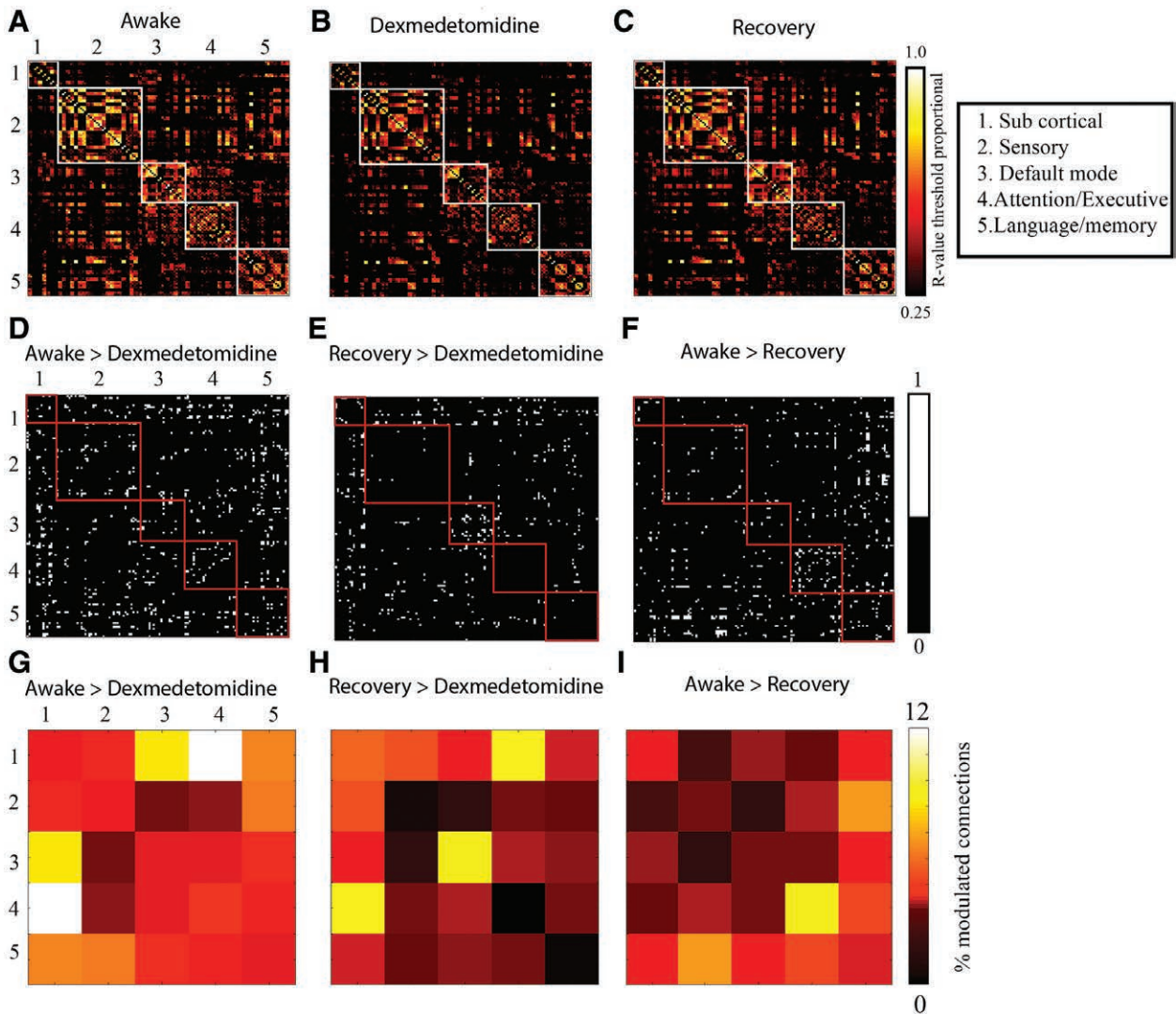
Fig. 3. Dexmedetomidine modulates within-network and between-network connections when networks are organized based on meta-analytic resting-state networks. (*A–C*) Adjacency matrices representing mean connectivity pattern in (*A*) awake, (*B*) dexmedetomidine, and (*C*) recovery states. The adjacency matrices consist of parcellation nodes ordered based on their membership in five resting-state networks listed in boxed legend. Resting-state networks were identified based on node overlap with connectivity maps in the neurosynth meta-analytic framework. (*D–F*) Contrast maps showing regions that significantly changed in connectivity within and between the five listed networks. Results are based on Student's *t* tests, where contrast shown in *D* is false discovery rate corrected at $P < 0.05$. (*E* and *F*) are uncorrected at $P < 0.01$. (*G–I*) Matrices showing percentage of nodes modulated in *D–F*. The percent values in *G*, *H*, and *I* are based on the sum of significantly modulated nodes observed in *D*, *E*, and *F*, respectively, scaled by the total number of possible connections.

partial restoration of connectivity within the default mode network and increased functional connectivity between subcortical regions and all other networks (fig. 3E; recovery > dexmedetomidine; uncorrected $P < 0.01$). Functional connectivity changes associated with dexmedetomidine did not fully revert to baseline values during the recovery state (fig. 3F; awake > recovery; uncorrected $P < 0.01$). The awake state, relative to the recovery state, had more within-network connectivity in attention/executive networks (fig. 3, F and I). Also, the language/memory networks had more between-network connectivity with subcortical regions, sensory network, default mode network, and attention/executive (fig. 3, F and I).

Discussion

We previously reported that impaired thalamic information processing—loss of functional connectivity between the default mode network and the thalamus and bidirectional changes between the frontoparietal networks and cerebellar clusters—is a neural correlate of dexmedetomidine-induced altered arousal.[1] In this investigation, we applied network metrics of information processing to study differences between baseline, dexmedetomidine-induced altered arousal, and recovery states. First, we found that dexmedetomidine reversibly reduced the local and global efficiencies of brain networks. Second, dexmedetomidine was associated with a reduction in

the mean strength of nodal connectivity but did not alter the relative distribution of connections between nodes. Third, by using a global network approach, we show that these changes are not specific to any given RSN. Taken together, these findings parallel the decreased efficiency of information transfer within the brain that has been reported for propofol-induced unconsciousness[17,30] and nonrapid eye movement sleep[18,19] and strengthen the hypothesis that conscious processing in the brain relies on an efficient system of information transfer.

The local and global efficiencies are both measures of information integration that are derived from the characteristic path length (the average shortest path length between all possible pairs of nodes).[31] Because the paths in this investigation represent statistical dependency or functional connectivity between nodes, our efficiency and mean node strength findings are consistent with our previous report of dexmedetomidine-induced functional connectivity changes.[1] Although our approach of representing each brain region in only one RSN based on the maximum overlap was different from the independent component analysis method we previously employed, our finding that functional connectivity was reduced between the default mode network and subcortical regions is also consistent with our previous report.[1] However, our current results extend upon those previously reported by showing that functional connectivity changes between subcortical regions are not specific to any RSN. Since sleep slow-delta (0.1 to 4 Hz) and spindle oscillations (13 to 16 Hz) reflect altered sensory information processing in the brainstem and thalamus,[32] it follows that dexmedetomidine-induced altered arousal, which is also associated with slow-delta and spindle oscillations,[33–35] should manifest with the altered subcortical–cortical functional connectivity. We speculate that other anesthesia-induced slow-delta oscillations (propofol, sevoflurane, and nitrous oxide),[34,36–40] Theta oscillations (4 to 8 Hz; ketamine and sevoflurane),[36,37] frontal alpha oscillations (8 to 12 Hz; propofol and sevoflurane),[34,36–40] and gamma oscillations (less than 40 Hz; ketamine)[41] may also manifest as altered subcortical–cortical and corticocortical fMRI BOLD network connectivity. A likely mechanism for this speculated finding is the disruption of *normal sensory processing* gamma oscillations (greater than 40 Hz) that have been related to fMRI BOLD signals.[42]

Recovery from the dexmedetomidine-induced altered arousal state was associated with partially recovered connectivity between brain regions that comprise the default mode network. Notably, within-network alterations in default mode network connectivity have been reported for dexmedetomidine,[1] sevoflurane,[43] propofol,[44] and ketamine.[45] Thus, this RSN, which is associated with stimulus-independent thought and self-consciousness,[46–48] may play a significant role in recovery from altered states of arousal. Our findings also suggest that key differences between the baseline and recovery states were increased within-network connectivity in attention/executive and language/memory networks. Thus, recovery from altered states of arousal may follow a graded pathway where within-network restoration of default mode functional connectivity precedes within-network connectivity in attention/executive and language/memory networks.

This finding, which suggests gradations in the level of arousal, is consistent with an information integration theory of consciousness.[9] It may result from time-varying disruption (altered arousal) or reintegration (recovery) of hub nodes.

Hubs are crucial for efficient information transmission in brain networks.[49] Although a detailed analysis of network hub dynamics was beyond the scope of this investigation, our finding of reduced strength of connectivity in highly connected nodes suggests that dexmedetomidine disrupts hub nodes. Importantly, a consistent finding from graph-theoretical studies of electroencephalogram[50] and rsfMRI[17,30] data during propofol-induced unconsciousness is the disruption of hub nodes. Further confirming the role of hubs in information transfer, a simulation of hub disruption using various anesthetics (propofol, sevoflurane, and ketamine) resulted in disrupted surrogates of information transfer.[51] This suggests that even though anesthetics have distinct pharmacologic targets—reflected by differences in behavioral states and oscillatory dynamics—preferential disruption of information flow at network hubs is a common *macrocircuit* dynamic. An open question is whether unique patterns of hub disruption may explain the pharmacologic and behavioral diversity inherent to these anesthetics.

A limitation of this study is that the level of arousal was not experimentally manipulated in a graded manner. Therefore, studies of dexmedetomidine and other anesthetics with graded manipulations of level of arousal levels are needed to more clearly delineate how the efficiency measures described in this article covary with the level of arousal. Another limitation of the current study is that the current results cannot be directly translated to molecular or neurophysiologic function at the neuronal level. We note that although statistically significant, our effect sizes were small in spite of clinically significant alterations to the level of arousal. However, this finding is likely a reflection of the mathematical construct underlying efficiency measures (*i.e.*, global and local efficiencies are not exponential functions).[10] Finally, it is important to note that the use of graph-theoretical metrics as a proxy for higher cognitive processes is not definitive.

Our findings demonstrate that dexmedetomidine is associated with a significant drop in the capacity for efficient information transfer in functional networks at both the local and global levels. These findings strengthen the hypothesis that conscious processing relies on an efficient system of information transfer in the brain.

Research Support

Competing Interests

The authors declare no competing interests.

Correspondence

Address correspondence to Dr. Hashmi: Dalhousie University, 4086, Pain Management Unit, 4th Floor Dickson Building, 5820 University Ave, Halifax, NS, Canada, B3H 1V7. javeria.hashmi@dal.ca. Information on purchasing reprints may be found at www.anesthesiology.org or on the masthead page at the beginning of this issue. Anesthesiology's articles are made freely accessible to all readers, for personal use only, 6 months from the cover date of the issue.

References

1. Akeju O, Loggia ML, Catana C, Pavone KJ, Vazquez R, Rhee J, Contreras Ramirez V, Chonde DB, Izquierdo-Garcia D, Arabasz G, Hsu S, Habeeb K, Hooker JM, Napadow V, Brown EN, Purdon PL: Disruption of thalamic functional connectivity is a neural correlate of dexmedetomidine-induced unconsciousness. Elife 2014; 3:e04499

2. Crick F, Koch C: A framework for consciousness. Nat Neurosci 2003; 6:119–26

3. Tononi G, Edelman GM, Sporns O: Complexity and coherency: Integrating information in the brain. Trends Cogn Sci 1998; 2:474–84

4. Hashmi JA, Davis KD: Effect of static and dynamic heat pain stimulus profiles on the temporal dynamics and interdependence of pain qualities, intensity, and affect. J Neurophysiol 2008; 100:1706–15

5. Hipp JF, Hawellek DJ, Corbetta M, Siegel M, Engel AK: Large-scale cortical correlation structure of spontaneous oscillatory activity. Nat Neurosci 2012; 15:884–90

6. Baars BJ, Gage NM: Cognition, brain, and consciousness: Introduction to cognitive neuroscience. Cambridge, Massachusetts: Academic Press, 2010

7. Buzsáki G, Draguhn A: Neuronal oscillations in cortical networks. Science 2004; 304:1926–9

8. Dehaene S, Changeux JP: Experimental and theoretical approaches to conscious processing. Neuron 2011; 70:200–27

9. Tononi G: An information integration theory of consciousness. BMC Neurosci 2004; 5:42

10. Achard S, Bullmore E: Efficiency and cost of economical brain functional networks. PLoS Comput Biol 2007; 3:e17

11. van den Heuvel MP, Stam CJ, Kahn RS, Hulshoff Pol HE: Efficiency of functional brain networks and intellectual performance. J Neurosci 2009; 29:7619–24

12. Buckner RL, Andrews-Hanna JR, Schacter DL: The brain's default network: Anatomy, function, and relevance to disease. Ann NY Acad Sci 2008; 1124:1–38

13. Loggia ML, Kim J, Gollub RL, Vangel MG, Kirsch I, Kong J, Wasan AD, Napadow V: Default mode network connectivity encodes clinical pain: An arterial spin labeling study. Pain 2013; 154:24–33

14. Hudetz AG: General anesthesia and human brain connectivity. Brain Connect 2012; 2:291–302

15. Bullmore E, Sporns O: The economy of brain network organization. Nat Rev Neurosci 2012; 13:336–49

16. Bullmore E, Sporns O: Complex brain networks: Graph theoretical analysis of structural and functional systems. Nat Rev Neurosci 2009; 10:186–98

17. Monti MM, Lutkenhoff ES, Rubinov M, Boveroux P, Vanhaudenhuyse A, Gosseries O, Bruno MA, Noirhomme Q, Boly M, Laureys S: Dynamic change of global and local information processing in propofol-induced loss and recovery of consciousness. PLoS Comput Biol 2013; 9:e1003271

18. Uehara T, Yamasaki T, Okamoto T, Koike T, Kan S, Miyauchi S, Kira J, Tobimatsu S: Efficiency of a "small-world" brain network depends on consciousness level: A resting-state FMRI study. Cereb Cortex 2014; 24:1529–39

19. Boly M, Perlbag V, Marrelec G, Schabus M, Laureys S, Doyon J, Pélégrini-Issac M, Maquet P, Benali H: Hierarchical clustering of brain activity during human nonrapid eye movement sleep. Proc Natl Acad Sci USA 2012; 109:5856–61

20. Correa-Sales C, Rabin BC, Maze M: A hypnotic response to dexmedetomidine, an alpha 2 agonist, is mediated in the locus coeruleus in rats. Anesthesiology 1992; 76:948–52

21. Nacif-Coelho C, Correa-Sales C, Chang LL, Maze M: Perturbation of ion channel conductance alters the hypnotic response to the alpha 2-adrenergic agonist dexmedetomidine in the locus coeruleus of the rat. Anesthesiology 1994; 81:1527–34

22. Nelson LE, Lu J, Guo T, Saper CB, Franks NP, Maze M: The alpha2-adrenoceptor agonist dexmedetomidine converges on an endogenous sleep-promoting pathway to exert its sedative effects. Anesthesiology 2003; 98:428–36

23. Jorm CM, Stamford JA: Actions of the hypnotic anaesthetic, dexmedetomidine, on noradrenaline release and cell firing in rat locus coeruleus slices. Br J Anaesth 1993; 71:447–9

24. Chiu TH, Chen MJ, Yang YR, Yang JJ, Tang FI: Action of dexmedetomidine on rat locus coeruleus neurones: Intracellular recording *in vitro*. Eur J Pharmacol 1995; 285:261–8

25. Biswal BB, Mennes M, Zuo X-N, Gohel S, Kelly C, Smith SM, Beckmann CF, Adelstein JS, Buckner RL, Colcombe S, Dogonowski A-M, Ernst M, Fair D, Hampson M, Hoptman MJ, Hyde JS, Kiviniemi VJ, Kötter R, Li S-J, Lin C-P, Lowe MJ, Mackay C, Madden DJ, Madsen KH, Margulies DS, Mayberg HS, McMahon K, Monk CS, Mostofsky SH, Nagel BJ, Pekar JJ, Peltier SJ, Petersen SE, Riedl V, Rombouts SARB, Rypma B, Schlaggar BL, Schmidt S, Seidler RD, Siegle GJ, Sorg C, Teng G-J, Veijola J, Villringer A, Walter M, Wang L, Weng X-C, Whitfield-Gabrieli S, Williamson P, Windischberger C, Zang Y-F, Zhang H-Y, Castellanos FX, Milham MP: Toward discovery science of human brain function. Proc Natl Acad Sci USA 2010; 107:4734–9

26. Hashmi JA, Kong J, Spaeth R, Khan S, Kaptchuk TJ, Gollub RL: Functional network architecture predicts psychologically mediated analgesia related to treatment in chronic knee pain patients. J Neurosci 2014; 34:3924–36

27. Kelly C, Toro R, Di Martino A, Cox CL, Bellec P, Castellanos FX, Milham MP: A convergent functional architecture of the insula emerges across imaging modalities. Neuroimage 2012; 61:1129–42

28. Yarkoni T, Poldrack RA, Nichols TE, Van Essen DC, Wager TD: Large-scale automated synthesis of human functional neuroimaging data. Nat Methods 2011; 8:665–70

29. Rubinov M, Sporns O: Complex network measures of brain connectivity: Uses and interpretations. Neuroimage 2010; 52:1059–69

30. Schröter MS, Spoormaker VI, Schorer A, Wohlschläger A, Czisch M, Kochs EF, Zimmer C, Hemmer B, Schneider G, Jordan D, Ilg R: Spatiotemporal reconfiguration of large-scale brain functional networks during propofol-induced loss of consciousness. J Neurosci 2012; 32:12832–40

31. Latora V, Marchiori M: Efficient behavior of small-world networks. Phys Rev Lett 2001; 87:198701

32. Steriade M, Contreras D, Amzica F: Synchronized sleep oscillations and their paroxysmal developments. Trends Neurosci 1994; 17:199–208

33. Akeju O, Kim SE, Vazquez R, Rhee J, Pavone KJ, Hobbs LE, Purdon PL, Brown EN: Spatiotemporal dynamics of dexmedetomidine-induced electroencephalogram oscillations. PLoS One 2016; 11:e0163431

34. Akeju O, Pavone KJ, Westover MB, Vazquez R, Prerau MJ, Harrell PG, Hartnack KE, Rhee J, Sampson AL, Habeeb K, Gao L, Lei G, Pierce ET, Walsh JL, Brown EN, Purdon PL: A comparison of propofol- and dexmedetomidine-induced electroencephalogram dynamics using spectral and coherence analysis. Anesthesiology 2014; 121:978–89

35. Huupponen E, Maksimow A, Lapinlampi P, Särkelä M, Saastamoinen A, Snapir A, Scheinin H, Scheinin M, Meriläinen P, Himanen SL, Jääskeläinen S: Electroencephalogram spindle

activity during dexmedetomidine sedation and physiological sleep. Acta Anaesthesiol Scand 2008; 52:289–94

36. Akeju O, Hamilos AE, Song AH, Pavone KJ, Purdon PL, Brown EN: GABAA circuit mechanisms are associated with ether anesthesia-induced unconsciousness. Clin Neurophysiol 2016; 127:2472–81

37. Akeju O, Westover MB, Pavone KJ, Sampson AL, Hartnack KE, Brown EN, Purdon PL: Effects of sevoflurane and propofol on frontal electroencephalogram power and coherence. ANESTHESIOLOGY 2014; 121:990–8

38. Lewis LD, Weiner VS, Mukamel EA, Donoghue JA, Eskandar EN, Madsen JR, Anderson WS, Hochberg LR, Cash SS, Brown EN, Purdon PL: Rapid fragmentation of neuronal networks at the onset of propofol-induced unconsciousness. Proc Natl Acad Sci USA 2012; 109:E3377–86

39. Pavone KJ, Akeju O, Sampson AL, Ling K, Purdon PL, Brown EN: Nitrous oxide-induced slow and delta oscillations. Clin Neurophysiol 2016; 127:556–64

40. Purdon PL, Pierce ET, Mukamel EA, Prerau MJ, Walsh JL, Wong KF, Salazar-Gomez AF, Harrell PG, Sampson AL, Cimenser A, Ching S, Kopell NJ, Tavares-Stoeckel C, Habeeb K, Merhar R, Brown EN: Electroencephalogram signatures of loss and recovery of consciousness from propofol. Proc Natl Acad Sci USA 2013; 110:E1142–51

41. Akeju O, Song AH, Hamilos AE, Pavone KJ, Flores FJ, Brown EN, Purdon PL: Electroencephalogram signatures of ketamine anesthesia-induced unconsciousness. Clin Neurophysiol 2016; 127:2414–22

42. Nir Y, Fisch L, Mukamel R, Gelbard-Sagiv H, Arieli A, Fried I, Malach R: Coupling between neuronal firing rate, gamma LFP, and BOLD fMRI is related to interneuronal correlations. Curr Biol 2007; 17:1275–85

43. Palanca BJ, Mitra A, Larson-Prior L, Snyder AZ, Avidan MS, Raichle ME: Resting-state functional magnetic resonance imaging correlates of sevoflurane-induced unconsciousness. ANESTHESIOLOGY 2015; 123:346–56

44. Boveroux P, Vanhaudenhuyse A, Bruno MA, Noirhomme Q, Lauwick S, Luxen A, Degueldre C, Plenevaux A, Schnakers C, Phillips C, Brichant JF, Bonhomme V, Maquet P, Greicius MD, Laureys S, Boly M: Breakdown of within- and between-network resting state functional magnetic resonance imaging connectivity during propofol-induced loss of consciousness. ANESTHESIOLOGY 2010; 113:1038–53

45. Bonhomme V, Vanhaudenhuyse A, Demertzi A, Bruno MA, Jaquet O, Bahri MA, Plenevaux A, Boly M, Boveroux P, Soddu A, Brichant JF, Maquet P, Laureys S: Resting-state network-specific breakdown of functional connectivity during ketamine alteration of consciousness in volunteers. ANESTHESIOLOGY 2016; 125:873–88

46. Raichle ME, MacLeod AM, Snyder AZ, Powers WJ, Gusnard DA, Shulman GL: A default mode of brain function. Proc Natl Acad Sci USA 2001; 98:676–82

47. Mason MF, Norton MI, Van Horn JD, Wegner DM, Grafton ST, Macrae CN: Wandering minds: The default network and stimulus-independent thought. Science 2007; 315:393–5

48. Vincent JL, Kahn I, Snyder AZ, Raichle ME, Buckner RL: Evidence for a frontoparietal control system revealed by intrinsic functional connectivity. J Neurophysiol 2008; 100:3328–42

49. van den Heuvel MP, Sporns O: Network hubs in the human brain. Trends Cogn Sci 2013; 17:683–96

50. Lee H, Mashour GA, Noh GJ, Kim S, Lee U: Reconfiguration of network hub structure after propofol-induced unconsciousness. ANESTHESIOLOGY 2013; 119:1347–59

51. Moon JY, Lee U, Blain-Moraes S, Mashour GA: General relationship of global topology, local dynamics, and directionality in large-scale brain networks. PLoS Comput Biol 2015; 11:e1004225